Electronic structure of solids using photoemission and x-ray emission spectroscopies

2001 J. Phys.: Condens. Matter 13 7885

(http://iopscience.iop.org/0953-8984/13/34/326)

INSTITUTE OF PHYSICS PUBLISHING JOURNAL OF PHYSICS: CONDENSED MATTER

J. Phys.: Condens. Matter **13** (2001) 7885–7904 PII: S0953-8984(01)25621-5

Electronic structure of solids using photoemission and x-ray emission spectroscopies

Esther Belin-Ferré

Laboratoire de Chimie Physique Matière et Rayonnement,
Université Pierre et Marie Curie—Centre National de la Recherche Scientifique,
Unité Mixte de Recherche 7614, 11 rue Pierre et Marie Curie, 75231 Paris Cedex 05, France

E-mail: belin@ccr.jussieu.fr

Received 8 June 2001, in final form 8 June 2001
Published 9 August 2001
Online at stacks.iop.org/JPhysCM/13/7885

Abstract

This paper aims to introduce briefly the underlying general principles of the photoemission and x-ray emission spectroscopy techniques. We summarize their principal characteristics and emphasize their complementarity for the investigation of the electronic structure of solids.

1. Introduction

Knowledge of the electronic structure of solids is of interest to better understand the physical and electronic properties and may allow us to clarify general trends in their behaviour; therefore, various theoretical as well as experimental means can be applied to analyse their band structure and densities of electronic states (DOS). It is the purpose of this paper to briefly present and compare two experimental x-ray spectroscopy techniques that give direct insight into the electronic structure of the occupied band of a material. They involve transitions between two quantum states of the solid, each one characterized by its lifetime and energy. These are x-ray photoemission and soft x-ray emission spectroscopies, denoted hereafter as PES and SXES, respectively.

For a few decades now, since the original work of Siegbahn and his co-workers, in Uppsala (Siegbahn *et al* 1967, 1969), photoemission spectroscopy (that they also labelled as ESCA: electron spectroscopy for chemical analysis) has become a world wide utilized technique as very efficient and powerful spectrometers are produced and marketed by various companies. In contrast, SXES is not so popular and no dedicated spectrometers are easily commercially available; they mostly have to be conceived and constructed with appropriate x-ray tubes in the laboratories where this technique is applied. However, nowadays SXES is going to get over a new step. Indeed, it is being developed by several groups, which operate home-made pieces of apparatus that use the very intense light beams of new generation synchrotron facilities to excite the x-ray spectra of materials (Ma *et al* 1992, Gallet *et al* 1998).

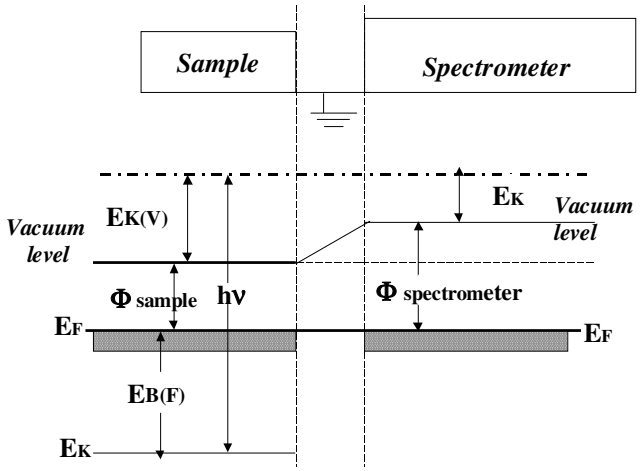

Figure 1. Scheme of the energy levels involved in binding energy measurements. E_F is the Fermi level, $E_{K(V)}$ is the kinetic energy with respect to the vacuum energy level of the sample whose work function is Φ_{sample}, $E_B(F)$ is the binding energy of the photoelectron created by the impinging photons and $\Phi_{spectrometer}$ is the spectrometer work function.

In the forthcoming sections 2 and 3 of this paper, the underlying general principles of the PES and SXES techniques are briefly introduced with attention paid to their principal characteristics and usefulness. In section 4 both techniques are compared and emphasis is put on their complementarity through a few selected examples.

2. Photoemission spectroscopy

Photoemission spectroscopy probes the kinetic energies E_K of photoelectrons emitted from inner levels of a solid or from the outermost occupied band (OB) as a result of the interaction of the solid with incoming x-ray (XPS) or ultra-violet (UPS) radiation of energy $h\nu$. Therefore, the initial state is the ground state of the system whereas there is a hole in the final state. In the framework of the frozen orbitals, thus assuming that the presence of such a hole in the final state does not affect significantly the remaining orbitals, the photoemission process involves three successive steps: (i) the excitation of the photoelectron, (ii) its travel through the sample and (iii) the ejection of the photoelectron into the vacuum. This last step depends on the photoelectron transmission probability.

Hence, the binding energy E_B of the photoelectron is related to its kinetic energy E_K by

$$E_K = h\nu - E_B - \Phi. \tag{1}$$

$h\nu$ is the energy of the incident photons beam and Φ denotes the difference between the work functions of the spectrometer and of the sample as schematized in figure 1.

Usually, the exact determination of Φ is not necessary provided the E_B scale is properly calibrated. This can be achieved by referring to a well known level such as the Au $4f_{7/2}$ level. For samples not prepared in clean high vacuum conditions, usually one takes as a reference the 1s level of contaminating carbon, always present at the surface of a sample. It is to note that whereas the Fermi levels of the spectrometer and metallic specimens adjust to each other, this no longer holds true for non-conducting substances. In such cases, charging effects can be observed. These induce shifts of the photoelectron peaks that can be as large as several eV. It is necessary to account for such displacements to correct measured E_B values.

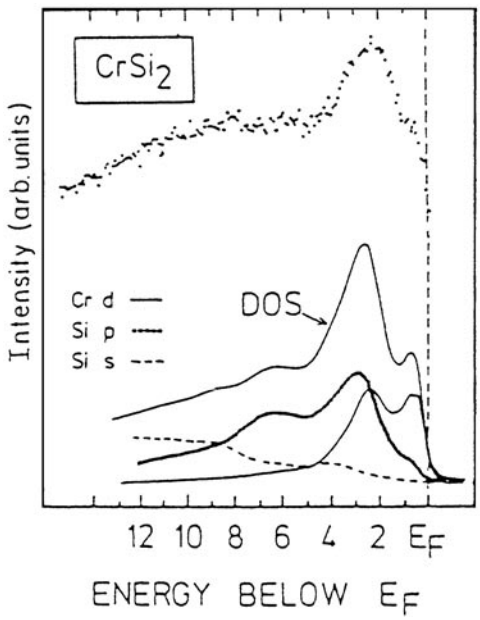

Figure 2. Integrated photoemission spectrum of $CrSi_2$ (dots). The solid line, indicated by an arrow, shows the total DOS reconstructed from partial DOS modulated by matrix elements and instrumental broadening. The dashed line is for Si s states, the dotted line is for Si p states and the thin full line is for Cr d states (Speier *et al* 1989).

There are two kinds of PES technique allowing us to explore final states. One is *integrated photoemission*, in which all possible final states contribute to the spectra. It is mainly applied to polycrystalline specimens. The binding energies of the various inner levels are obtained separately whereas, for the OB, the contributions of all the electrons are summed, each one modulated by the corresponding photoelectron cross sections σ. The experimental data are usually compared to total DOS calculations. Such comparison is made more meaningful by convoluting the theoretical DOS with appropriate functions in order to account for the photoemission cross sections and experimental functions (figure 2).

The other technique is *angle resolved photoemission*, which applies to single crystals. In this technique, the damping of the escaping photoelectrons is weak enough so that only transitions with k momentum conservation are detected. Accordingly, the energy dispersion curves of the material can be investigated, which informs us about the band structure topology as well as Fermi surfaces. The data are often treated using the free-electron final state model and the experimental results are compared to band structure calculations (figure 3). This technique is also labelled ARUPS or ARXPS according to whether the incoming photons are ultraviolet radiation or x-rays. The final energy resolution of the PES measurements depends upon the natural energy width of the incident photon beam and the spectrometer experimental function. For XPS it is generally about 0.4–1 eV and for UPS it may be as good as a few tenths of an eV.

Within the framework of the time dependent perturbation theory and the dipole approximation, that suppose the incident radiation is non-polarized and the final state is not degenerate, the photoemission cross sections are written

$$\sigma(h\nu) = (1/4\pi\varepsilon_0)(4\pi^2/3)(\mathrm{e}^2/\hbar c)h\nu|\langle\psi_f|r|\psi_i\rangle|^2 \tag{2}$$

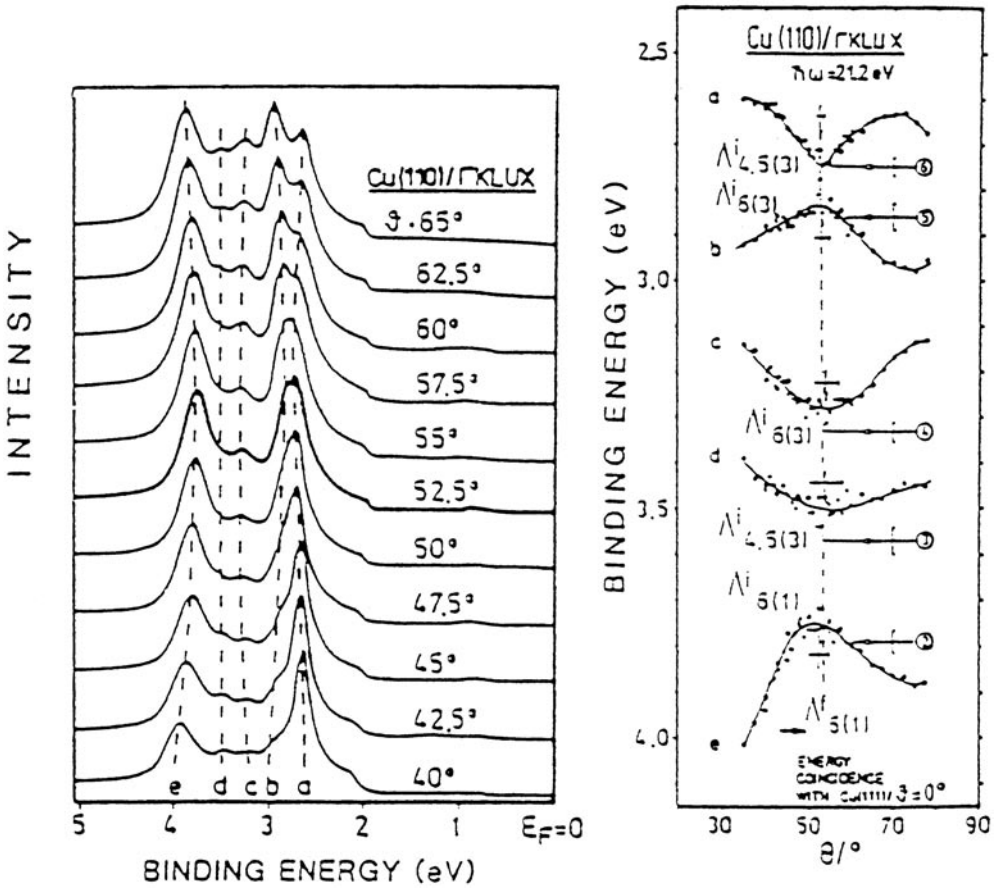

Figure 3. ARUPS spectra of Cu (110) in the GKLUX plane. In the left panel, the UPS spectra are taken at 21.2 eV incident energy for different detection angles. The right panel shows the curves corresponding to features a to e of the ARUPS spectra as a function of the detection angle. These curves have to be compared to calculations (see for instance Burdick 1963).

where ψ_f and ψ_i are the wave functions of the final and initial states, respectively, and r is the position of the electron. Hence, $\sigma(h\nu)$ highly depends on the incoming photon energy. The trends in the variation of $\sigma(h\nu)$ are similar in metallic specimens and pure elements (Rossi *et al* 1983, Cole *et al* 1992). Therefore, one can achieve some site selectivity and distinguish between the features due to separate contributions to the OB of an alloy or compound, provided the respective photoionization cross section values are different enough, by tuning the incident energy. An illustration is given in figure 4(a), which shows PES spectra of icosahedral $Al_{65}Cu_{20}Os_{15}$ for different incident photon energies (Zhang *et al* 1995). Note that the photoionization cross section for the Os 5d sub-shell is a maximum around 35 eV whereas for Cu 3d the maximum is around 50 eV (Yeh 1993). Figure 4(b) also shows the spectra for decagonal $Al_{70}Co_{15}Ni_{15}$ (Stadnik *et al* 1995). Here, the photoionization cross sections for the Ni 3d and Co 3d sub-shells are too close to allow for discerning features induced by Ni and Co d states on the OB spectra. Furthermore, the photoemission cross sections significantly favour d and f states as compared to p or s states (Yeh and Lindau 1985, Yeh 1993). As a consequence, no features arising from sp constituents are observed in the OB spectra of specimens made of sp as well as d and f elements.

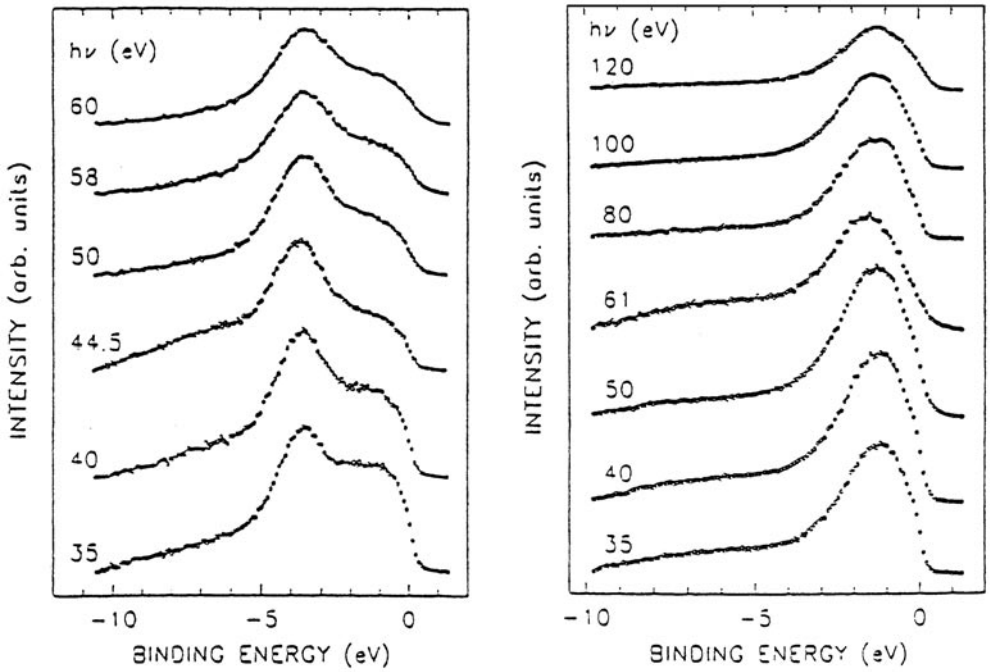

Figure 4. Valence bands of icosahedral $Al_{65}Cu_{20}Os_{15}$ (left panel) and of decagonal $Al_{70}Co_{15}Ni_{15}$ (right panel) for different incident photon energies.

During its travel through the solid, the photoelectron undergoes inelastic interactions by the electrons of the medium. So, the sampled depth is governed by the mean free path of the photoelectrons, denoted Λ. Therefore, PES is basically a surface-sensitive technique that generally probes thickness up to 3Λ. This makes it necessary to very carefully prepare and characterize the surfaces of the specimens under study.

In the spectra of solids, the photoelectron peaks are superposed to a background that is not a simple function because of the inelastic interactions with the electrons of the medium, especially important if the sample is a good conductor. In that case, there is an asymmetric broadening of the valence peak towards low E_K. Therefore, to analyse the spectra it is necessary to account for an attenuation length that depends on E_K. It has been shown to be lower for E_K between 30 to 100 eV, that corresponds to the UPS energy range; accordingly, UPS is the most sensitive to the surface. For energies above a few hundreds of eV (XPS energy range), the attenuation length is proportional to $E_K^{0.52}$ (Powell 1974, Lindau and Spicer 1974).

The intrinsic shape of the energy distributions of a core-level peak is a Lorentzian curve whose full width at half maximum intensity (FWHM), $\Delta E_{n,\ell,j}$, depends on the lifetime τ of the inner hole through

$$\Delta E_{n,\ell,j} = \hbar\tau^{-1}. \tag{3}$$

The core-level spectra are superposed on an asymmetric background that originates from the immediate response of the system to the photohole of the final state but, in narrow energy ranges, a linear background is often subtracted from the raw data. Then, the core-level spectra are decomposed into Lorentzian curves and compared to standards (figure 5). Actually, for meaningful decompositions, Voigt functions can also be used, since it is commonly admitted that the experimental function of the PES spectrometer is a Gaussian distribution.

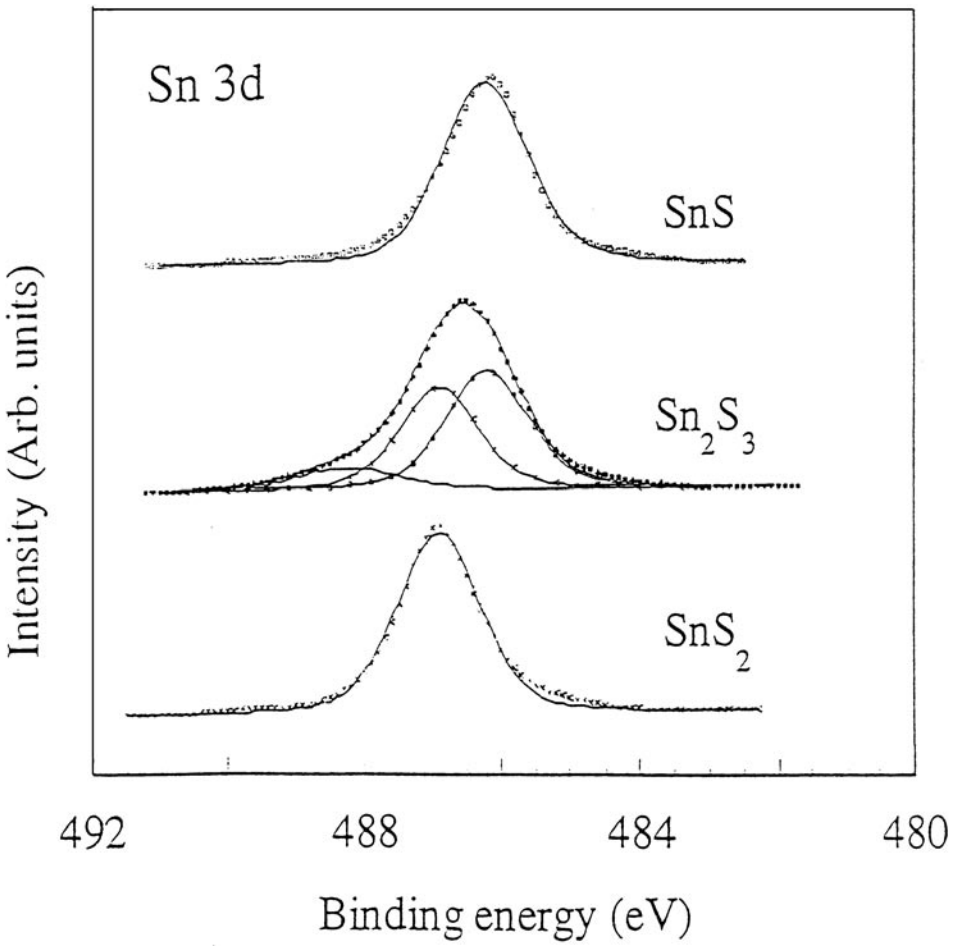

Figure 5. Sn 3d spectra in SnS, SnS_2 and Sn_2S_3. The experimental peaks (dots) are adjusted to Lorentzian curves (solid lines). Note that for the latter compound, the Sn peak can be decomposed into two contributions at the energies of the peaks in SnS where the Sn has the valency 2+ and in SnS_2 where the valency of Sn is 4+. This shows that both oxidation degrees of Sn are present in Sn_2S_3. The additional contribution arises from oxidation of the specimen (Gheorghiu de La Rocque *et al* 2000).

The number $\mathcal{N}(h\nu)$ of emitted photoelectrons can be expressed as a function of the number of incident photons of energy $h\nu$, $n(h\nu)$, the DOS at initial and final states $N(\varepsilon)_i$ and $N(\varepsilon)_f$, respectively, the Fermi–Dirac temperature function f_{FD}, the photoemission cross section, $\sigma(h\nu)$, and the instrumental detector transmission efficiency, $A(h\nu)$, that also depends on the acceptance solid angle of the analyser. Accordingly,

$$\mathcal{N}(h\nu) \propto n(h\nu)N(\varepsilon)_i N(\varepsilon)_f f_{FD}\sigma(h\nu)A(h\nu)\Lambda(1 - \exp -x/\Lambda\cos\theta). \qquad (4)$$

So, the contribution to the total intensity due to an element M at a depth x in a direction referred to by its angle θ with the surface of the sample is related to its concentration and to the electron's mean free path. Therefore, accurate measurements of the intensity of a specific core level of a given element in a sample make it possible to determine its concentration by comparing the intensities of the same photoelectron peak in the specimen and the pure element.

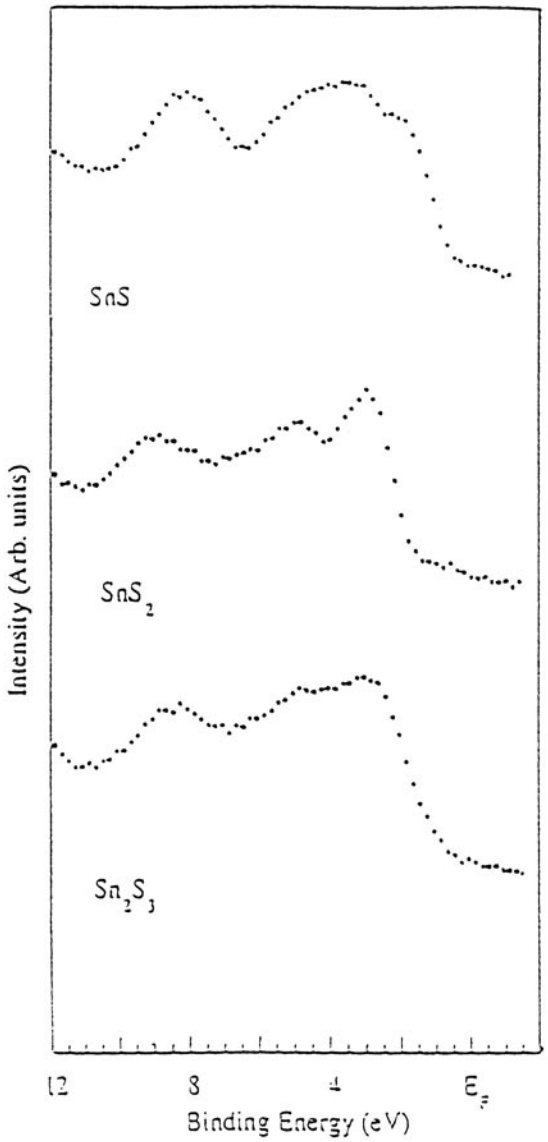

Figure 6. Valence bands of SnS, SnS_2 and Sn_2S_3. The shape of the valence band for Sn_2S_3 is intermediate between those of SnS and SnS_2 (Gheorghiu de La Rocque *et al* 2000).

Profile variations of the concentration of an element M in a sample can be achieved by measuring the intensities of a chosen inner level peak with tuning the angle θ. This one should differ from the grazing-incidence angle. Indeed, in this case, diffraction of the incoming x-rays by the surface of the sample may modify the way the incident radiation is attenuated. Hence, the PES technique is of importance from both chemical qualitative and quantitative standpoints.

Investigation of the PES core-level spectra is useful not only because it carries qualitative and quantitative information but also because inner levels are very sensitive to the chemical environment. Shape modifications (for example, broadenings in amorphous systems as compared to crystals) as well as shifts up to a few eV (usually less than 5 eV) with respect to

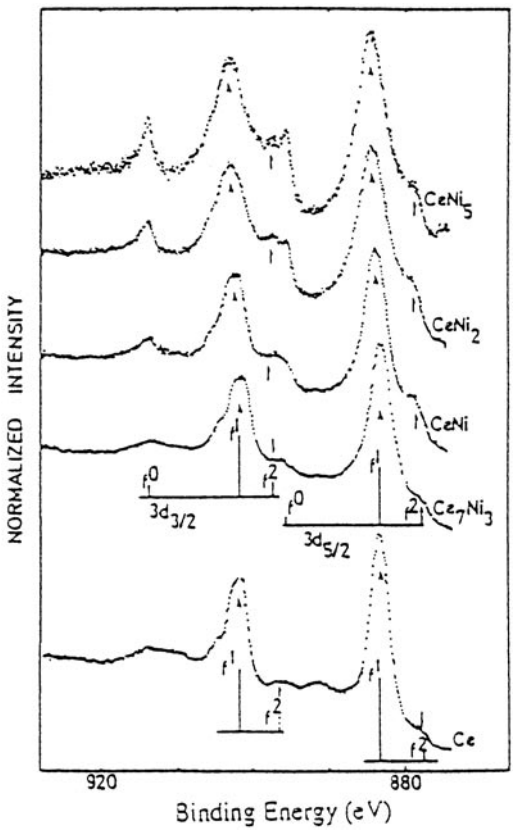

Figure 7. Ce 3d XPS spectra in a series of ordered Ce–Ni intermetallics. Note the growth of the peak due to the f^0 configuration with increasing Ni content in the sample (Fuggle 1983).

pure elements can be observed from sample to sample. Indeed, the energy of an electron in a core level depends on the attractive potential of the nucleus of the atom and the repulsive interaction due to the other electrons that surround it. During the photoemission process, all the orbitals of the system participate in the screening of the hole. The screening energy contributes to lower the energy of the system; it usually amounts to less than 10% the binding energy. It involves two terms: one is due to the intra-atomic relaxation of the electronic cloud of the perturbed atom itself and the other term comes from the relaxation of neighbour atoms. Therefore, the energy of an electron in a core level is affected by any change of the potentials to which it is subjected whatever the reason: changes in chemical bonds or in the atomic state (allotropy) (figure 5).

To account exactly for core-level shifts requires reference to models. These involve relaxation energy terms, electronegativities, formation enthalpies etc. Accordingly, investigation of the so-called 'chemical shifts' is of great interest, as it enlightens us on the chemical state of the element under study. These changes in the atomic or chemical environments also induce modifications of the distribution of the valence electrons and, consequently, core levels shifts are observed at the same time as variations of the shapes of valence bands (figure 6).

Aside from core-level or OB peaks, the photoelectron spectra also display additional features that arise from characteristic energy losses and Auger as well as shake-up and shake-off processes, plasmon excitations, surface state contributions etc and also final-state effects.

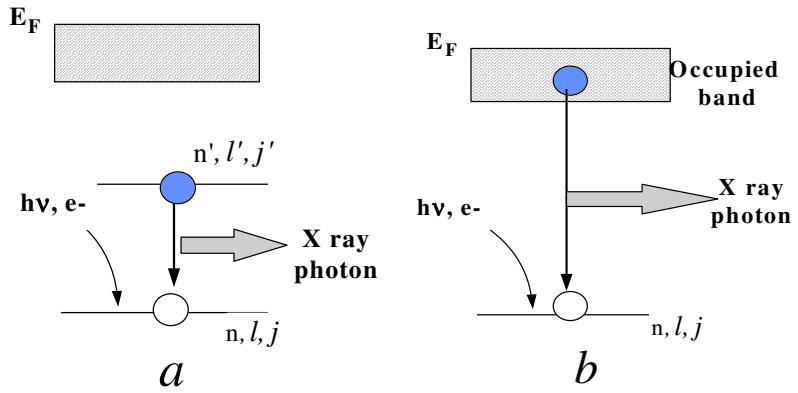

Figure 8. (a) The x-ray transition to between two inner levels of the solid; (b) the x-ray transition involving a core level and the occupied band.

Plasmon excitations are found towards high E_B of the peaks, whereas surface states give contributions to the low E_B side. Final-state effects usually do not dominate in the spectra except for elements with unfilled inner shells, like the 4f levels of rare earths. Then, the photoemission spectra display a number of complex features and/or multiplets involving f^n, f^{n+1} and f^{n+2} final-state configurations (figure 7).

More details on the PES techniques can be found in many textbooks, for instance in Barr (1993), Brundle and Baker (1978), Cardona and Ley (1978, 1979) or in Hüfner (1995) etc.

3. X-ray emission spectroscopy

An ionized or excited system is not stable and evolves spontaneously. Hence, a hole in a core level of a solid fills from either a more external level, or the OB. Such a recombination can be either radiative or non-radiative. The radiative process is the x-ray emission that leaves a hole in their outermost occupied band. The non-radiative counterpart is the Auger effect, not treated here, which ends up emitting one electron (core electron or from the OB) and leaving two holes in the final state.

In an x-ray emission process, the energy of the emitted photon is the difference between the energies E_i and E_f of the initial and final states, respectively. These transitions are investigated by means of the x-ray emission spectroscopy (XES) technique. Within the one-electron approximation, thus neglecting relaxation energy terms, the x-ray emission involves two steps: the first one is the creation of the inner hole at level $\mathcal{L}(n, \ell, j)$ and the second is the reorganization of the electronic cloud from another level $\mathcal{L}(n', \ell', j')$ or from the OB. This is schematized in figures 8(a) and (b).

The energy distribution of the emitted radiation for a transition involving two levels, $\mathcal{L}(n, \ell, j)$ and $\mathcal{L}(n', \ell', j')$ or one level and the OB, respectively, are given by relations (5) and (6):

$$I_{(h\nu)} \propto |M_{f\to i}|^2 \mathcal{L}(n', \ell', j')^* \mathcal{L}(n, \ell, j) \tag{5}$$

$$I_{(h\nu)} \propto |M_{f\to i}|^2 N(\varepsilon)^* \mathcal{L}(n, \ell, j). \tag{6}$$

$M_{f\to i}$ is the matrix element of the transition probability; it is constant or varies slowly with energy; it depends on $|\langle \Psi_f | r | \Psi_i \rangle|$, where Ψ_i and Ψ_f are the wave functions of the initial and final states, respectively. In (5), the initial and final states are highly localized; in contrast,

in (6), Ψ_i is a localized state whereas Ψ_f is more extended-like in character as it describes a hole in the OB; note that here $N(\varepsilon)$ represents the probed OB densities of states.

For a transition to take place, it is necessary that Ψ_i and Ψ_f overlap. This requirement means that only the amplitude of Ψ_f in the core hole region will contribute significantly to the transition. As a consequence, XES possesses a local character. It is also necessary that the radiative transition probability differs from 0, which is achieved provided dipole selection rules are satisfied, namely

$$\Delta\ell = \pm 1 \qquad \Delta j = 0, \pm 1. \tag{7}$$

Hence, if a core hole with symmetry ℓ is created in an element, alone or in a compound, the local density of states with $\ell \pm 1$ symmetry around this element, denoted by $N(\varepsilon)^{\ell\pm1}$, will be probed by the XES technique. This gives a partial character to XES. Consequently, comparison of the experimental XES spectra with partial densities of states calculations is possible. However, it is to note that transitions with $j' = 0 \rightarrow j = 0$ are not allowed and that transitions to $\ell + 1$ states are favoured with respect to those to $\ell - 1$. Accordingly, for transitions involving an inner hole of p symmetry, recombination from d-like states will have a much higher probability than that from s-like states. More details can be found in textbooks, such as Agarwal (1979), or in Bonnelle (1987).

In the framework of the frozen orbitals, the shape of the intensity distribution for a transition involving two inner levels is a Lorentzian curve whose FWHM is the sum of the FWHMs of the Lorentzian distributions attached to the levels participating in the transition. Its energy is the difference between the energies of the orbitals corresponding to the final and initial states. Indeed, the relaxation energy due to the screening of the inner hole does not vary significantly from one inner level to another one and therefore is not seen in the difference between the corresponding energy levels. However, this does not hold true for open shells, especially f shells. As the initial state of XES is the same as the final state in PES, one expects many features are observed on the emission spectral distribution curves, which arise from final-state effects. In the one-electron approximation, the emitted intensity distribution for a transition involving OB states results from the convolution of the probed partial local DOS and the Lorentzian distribution $\mathcal{L}(n, \ell, j)$. Here again, whereas the final hole in the OB can generally be well accounted for by an extended wave function, this is no longer true for transitions involving d and f states.

The total energy resolution of an experiment depends on the natural width $\Delta E(n, \ell, j)$ of the inner level $\mathcal{L}(n, \ell, j)$ and the instrumental function $\Delta E(n, \ell, j)$ varies from a few meV up to several eV according to the atomic number and level considered (Krause and Oliver 1979). It is generally the most important parameter in the selection of the appropriate transitions to investigate. Therefore, no absolute DOS values are obtained from XES measurements. However, it is possible to compare the DOS of a given element in various materials. Indeed, according to relation (6), any change in the shape and energy of the spectral distributions will give direct insight into modifications of the corresponding $N(\varepsilon)$. An example is given in figure 9 for the Al 3p state distribution in fcc Al and in Al_2Cu. The shape of the distribution in the alloy departs from the parabolic-like shape as in pure fcc Al, which shows it is not a free-electron-like intermetallic. The dip in the middle of the distribution is due to the interaction between Al 3p and Cu 3d states (Fournée *et al* 1998).

The XES technique is straightforward. It is directly applicable to any kind of material: crystalline, amorphous, insulator, bulk, powder etc. According to the incident energy, it makes it possible to probe bulk states, states at deep interfaces or superficial layers. Whatever the technique applied to create the initial state, namely irradiating the sample with impinging electrons or photons (this latter technique is the so-called fluorescence technique and can be

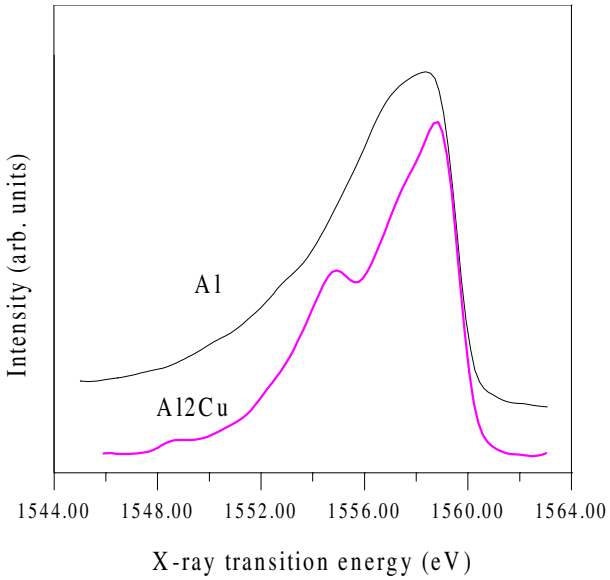

Figure 9. Al 3p state distribution in pure fcc Al and in crystalline Al_2Cu. The dip in the middle of the curve for Al_2Cu is due to the interaction with Cu d states (Fournée *et al* 1998).

used at synchrotron facilities), multiple interactions may take place and, accordingly, satellite emissions may be observed on the spectra. These are due to the x-ray transition in the multiple ionized or excited system and to shake-up and shake-off or Auger processes as well as to plasmon energy losses. To minimize the satellite contribution due to multiple ionizations or excitations it is worth irradiating the system with incoming particles of energy close to the threshold transition energy. This also avoids modifications of the spectra due to reabsorptions of the emitted x-ray radiation into the sample itself. Such reabsorption effects may be very strong and responsible for artifacts on the spectral distributions as shown in figure 10 for the 3d–4f emission in Ce excited with incident electrons of increasing energies, therefore involving increasing sampled depth and accordingly larger reabsorption through the emissive thickness.

It is important to underline that in XES, the contributions of the various components to the OB of a solid can be investigated separately whatever they are and comparison with partial DOSs is meaningful. However, each curve is obtained in its own transition energy scale and is normalized to its own maximum intensity. To achieve a picture of the OB and have insight into all the electronic interactions that are present, further adjustment of the various partial contributions in the energy scale is necessary. For such a purpose, one has to set the Fermi energy E_F onto each individual x-ray transition energy scale. This requires us to determine the binding energy with respect to E_F of the inner level participating in each x-ray transition and can be done thanks to complementary x-ray and (or) inner-level PES measurements. An example is shown in figure 11, again for Al_2Cu. The probed transitions describe the Al 3p, Al 3s,d and Cu 3d–4s states. Note that transition probabilities strongly favour d states. So, although the proportion of Al d states is very small with respect to Al s states, these are seen whereas no information on the Cu 4s states is obtained experimentally.

Of course, such an adjustment is not necessary if one compares only the variation of selected states in various solids; then spectra can be given directly in the x-ray transition energy scale.

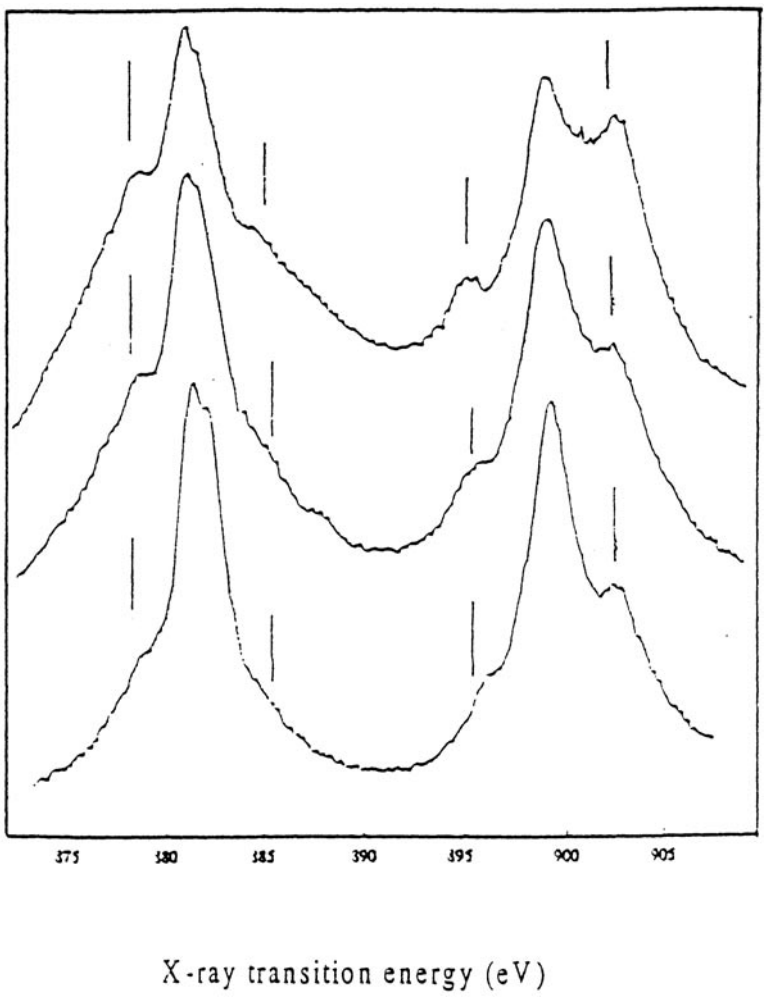

Figure 10. Ce 4f–3d emission in metallic Ce taken at energies of 1600 eV (bottom curve), 1900 eV (middle curve) and 2500 eV (top curve) respectively. Note the progressive increase of intensity of the structures indicated by the vertical ticks and decrease of the intensity of the principal line with increasing excitation energy (Sonder 1990). The onset of peaks at the left is the Ce $3d_{3/2}$ inner level and the onset on the right is for Ce $3d_{5/2}$.

As mentioned, for samples containing elements with open shells, many features are observed on the emission spectral distribution curves, which arise from final-state effects due to both ionized and excited configurations (see figure 7). Each of these configurations is involved in the x-ray transition so that many features that involve $3d^9 4f^1$, $3d^{10} 4f^0$ and $3d^9 4f^2$ configurations are present in the x-ray spectra. This is exemplified in figure 12, that shows the Ce 4f–3d emission spectrum in $CeNi_2$. This intermetallic is actually a mixed valence alloy and structures characteristic of both Ce^{3+} and Ce^{4+} are observed on the spectral distribution curve (Sonder 1990).

The one electron picture is a simple model to describe the x-ray emission technique and applies well to solids that are investigated with excitation energies about 1.5 times that of the probed threshold. More elaborate models that account for core hole effects when going closer to threshold energies can be successfully used.

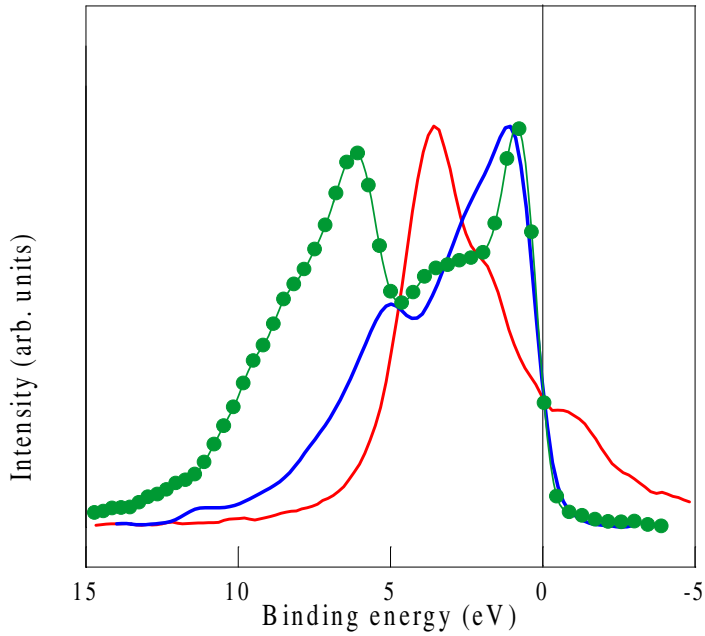

Figure 11. Electronic distributions of the occupied band of Al_2Cu as plotted in the binding energy scale. Cu 3d states correspond to the solid line, Al 3p states are displayed as the thick solid line and the Al 3s–d states are shown as the thin line with symbols (Trambly de Laissardière *et al* 1995).

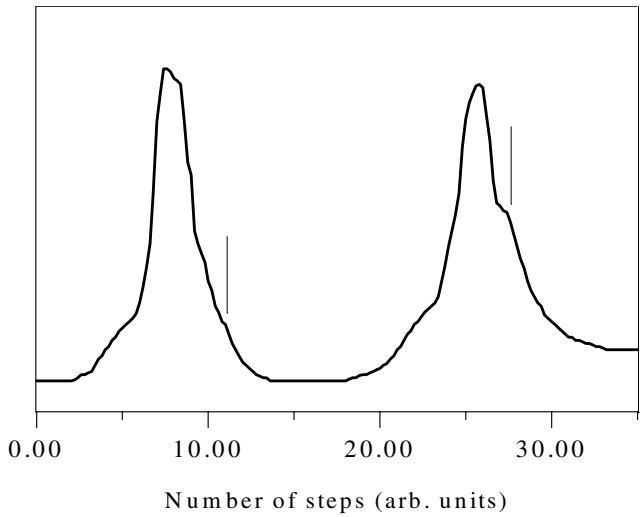

Figure 12. Ce 4f–3d emission in $CeNi_2$ intermetallic. The vertical ticks show the features that correspond to Ce^{4+} whereas the other structures refer to Ce^{3+} (Sonder 1990).

As an example let us mention the investigation of C K edge densities of states of a freshly cleaved pyrolitic sample in order to probe C p states (Ma *et al* 1992, Carlisle *et al* 1999) as measured recently at ESRF (European Synchrotron Research Facility). On the spectrum taken with incident energy below the C 1s level, inelastic loss features were observed, which

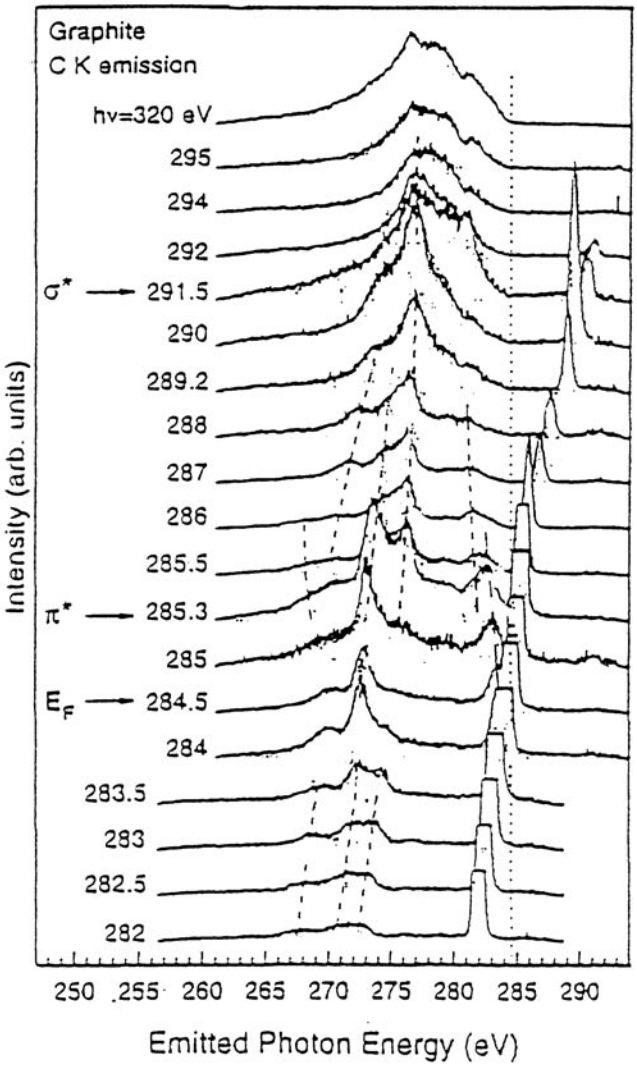

Figure 13. C K x-ray fluorescence emission spectra of pyrolotic graphite. The C 1s states are probed with energies increasing from 282 to 320 eV in order to excite below and far above the C is core level. The isolated peak on the right side of the curves is the elastic peak (Carlisle *et al* 1999).

disperse linearly with excitation energy. Just above the threshold, features do not move linearly (figure 13). However both behaviours could be interpreted using the same theory for resonant fluorescence and the authors showed that the variations observed in the emission spectra are related to changes in the absorption cross sections. Note that the changes are more significant for excitations above the C 1s level because of the multiplicity of the core excited state being probed. The authors also concluded that resonant fluorescence spectroscopy, namely tuning the energy through a threshold, although requiring quite heavy theoretical support can be successfully utilized to investigate the band structure of solids.

Another example of the usefulness of x-ray fluorescence spectroscopy using synchrotron radiation is provided by the study of magnetic circular dichroïsm. This was done with a

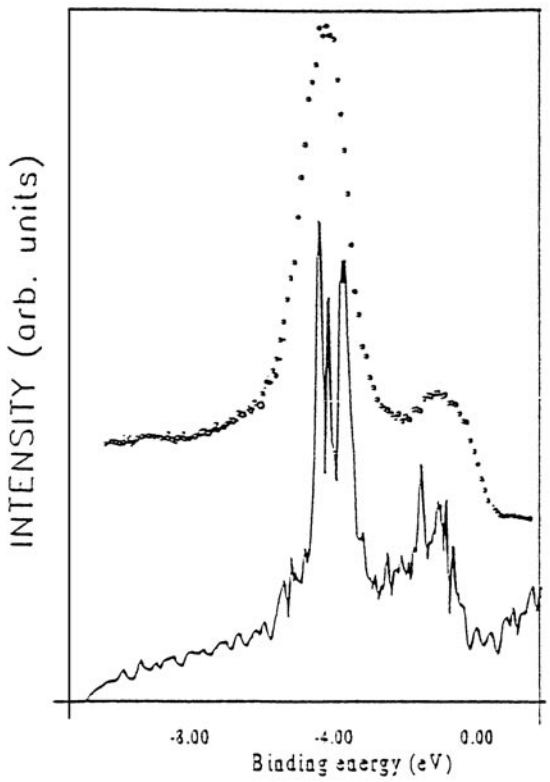

(a)

Figure 14. (a) Comparison between the PES spectrum of Al_7Cu_2Fe (Stadnik and Stroink 1993) and calculated total DOS (Trambly de Laissardière *et al* 1995). The onsets of peaks centred around 4 eV and 2 eV below the Fermi energy arise from Cu 3d states and Fe 3d states, respectively. (b) Comparison between the XES spectra of Al_7Cu_2Fe adjusted in the binding energy scale and the corresponding calculated partial DOS. Because the experiment reflects transitions from both s and d states of the valence band to the inner level of symmetry p, the top panel shows the calculated Al s (thick solid line) and Al d (thin solid line) partial DOSs. For Cu and Fe, the 4s calculated counterparts are not shown as the transition probabilities mean that the s states do not contribute significantly to the measurement (see the text) (Trambly de Laissardière *et al* 1995).

circularly polarized beam at the ring storage of the LURE (Laboratoire pour l'Utilisation du Rayonnement Electromagnétique), by Hague *et al* (1993) from Fe $L_{2,3}$ measurements and more recently by Gallet *et al* (1998) from Rh 4d state studies in Co–Rh alloys.

4. Complementarity of PES and XES techniques

As PES provides a view of the total OB and XES gives the partial contributions, it may be interesting to combine both techniques for a better understanding of the electronic structure of a solid. We give here three examples among the data published so far. The first one refers to crystalline Al_7Cu_2Fe.

Figures 14(a) and (b) present PES and XES spectra as well as calculated DOS curves. For such an intermetallic, total and partial DOS calculations performed with the linearized muffin tin orbitals (LMTO) method are available (Trambly de Laissardière *et al* 1995). Therefore,

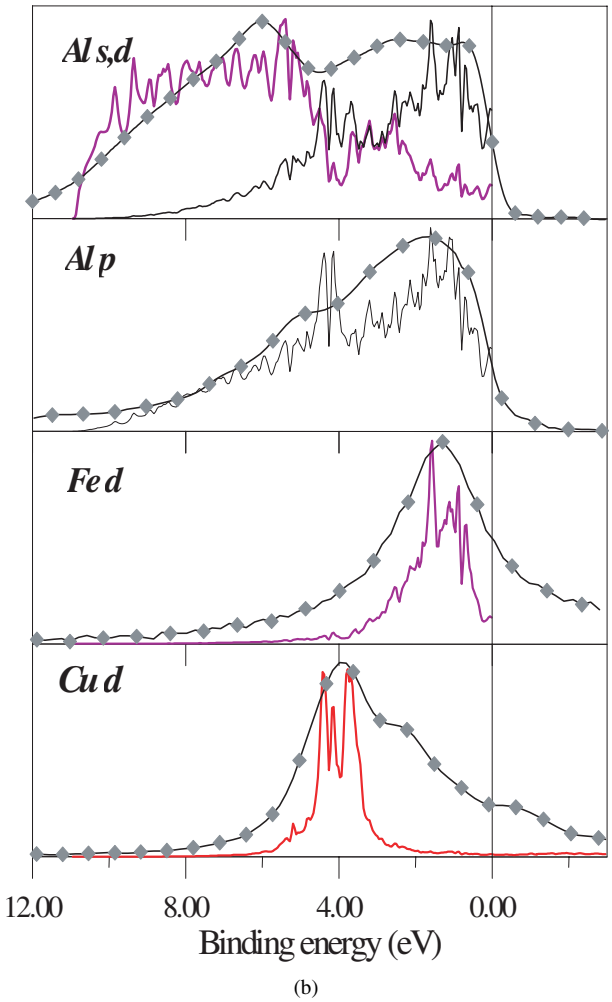

(b)

Figure 14. (Continued)

direct comparison of both experimental and calculated data is possible. This furthermore shows good agreement (figure 14(a)). The PES measurements ascertain that Cu states are dominant in the DOS and show Fe states are located not far from E_F. The XES experiments complemented by Al, Cu and Fe inner level binding energy measurements show the Al–Cu and Al–Fe interactions and point out significant hybridization between Al 3p and Fe 3d states close to E_F (figure 14(b)). The probed x-ray transitions are Al $L_{2,3}$, that describes 3s–d states (transitions from the valence band to the Al 2p holes), Al Kβ, that probes 3p states (transitions from the valence band to the Al 1s hole), and both Cu Lα and Fe Lα (transitions from the valence band to Cu $2p_{3/2}$ and Fe $2p_{3/2}$, respectively). Such a type of comparison has been used in the study of quasicrystals to validate DOS calculations performed for model approximants (Belin-Ferré *et al* 1996, Krajci *et al* 1995). These latter are crystalline structures, usually with huge unit cells, whose local order is similar to that of the parent quasicrystal.

The second example is provided by the investigation of $TiSi_2$. The data allow us to obtain a detailed picture of the various contributions to the occupied band (valence band) as displayed

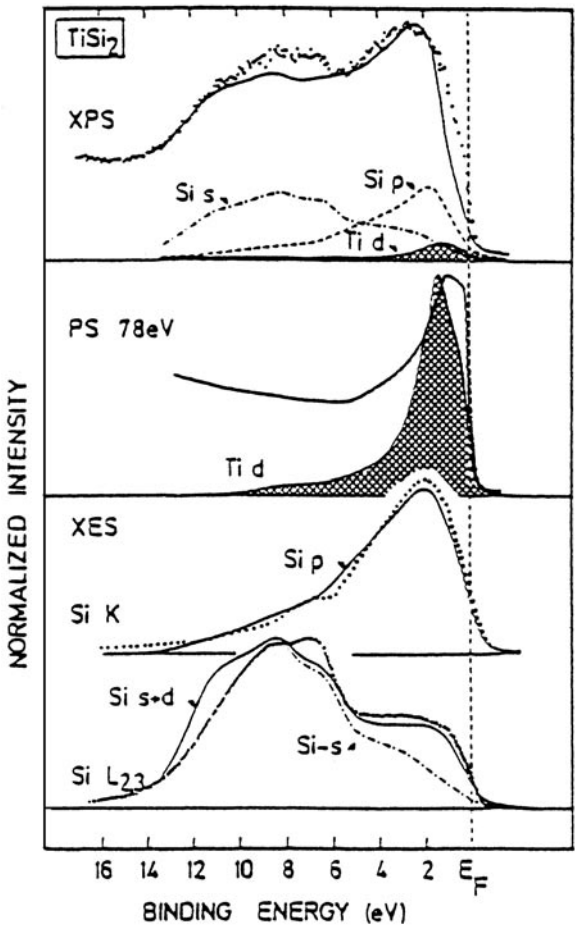

Figure 15. Comparison of calculated and experimental valence electronic states in $TiSi_2$. The calculated spectra are the full lines. They are obtained by including matrix elements in the theoretical DOS. For Ti only d states are shown as these are the states that contribute significantly to the results as obtained from experiments. Note that in the XPS spectrum (top panel) the Ti d states are seen as a shoulder near the Fermi energy due to low photoionization cross section whereas in the upper middle panel, the UPS spectrum mainly reflects the metal d character. The two lower panels depict the Si 3p and Si 3s,d states respectively.

in figure 15. Such a study ascertains that whereas extended-like states of Si are found far below the Fermi level, Ti–Si hybridized states are present in an energy range that extends over about 3 eV from the Fermi level. These are Ti 3d states that overlap Si 3p states (Weijs *et al* 1990). The XPS involves all the valence band states whereas the one taken at 78 eV (Weaver *et al* 1984) mainly reflects the Ti d states. The calculated DOSs were broadened in order to account for core level lifetime. Note that the Si d DOS was divided by 2 and added to the Si s calculated counterpart in order to improve agreement with the Si $L_{2,3}$ experimental curve (transition from the valence band to the Si $2p_{1/2}$ and Si $2p_{3/2}$ inner levels).

The last example refers to the decagonal Al–Co–Ni quasicrystal, whose valence band as obtained from PES measurements is shown in figure 4, right panel. Various models have been elaborated based on clusters to represent the atomic structure of the orthorhombic approximant

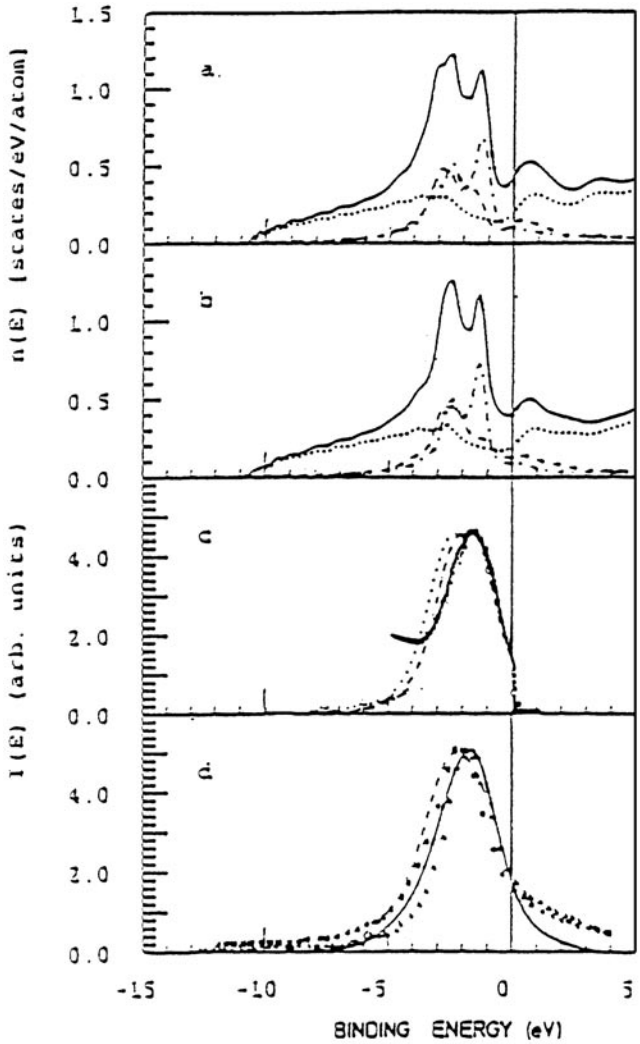

Figure 16. Total and partial DOS curves (panels a and b) of the orthorhombic approximant of the decagonal quasicrystal Al–Co–Ni with different cluster arrangements (Krajci *et al* 2000). Panel c compares the calculated photoemission intensities deduced for the two structural arrangements (dotted and dashed lines, respectively) with PES data from Stadnik *et al* (1997) (thick line). Panel d shows the calculated partial SXES Co 3d (dashed line) and Ni 3d (full line) sub-bands curves, respectively, that are compared with SXES experimental spectra for Co 3d (squares) and Ni 3d (triangles) from Fournée (1998).

to these decagonal phases, which involve various Co, Ni, Ni–Al and Ni–Co rings and DOS calculated by the TB-LMTO method on the basis of these models. Comparison has been made with PES as well as SXES data. This is shown in figure 16 (Krajci *et al* 2000). The two upper panels, a and b, show the total and partial Ni, Co and Al DOS for two different atomic arrangements. In panel c, photoemission intensities have been calculated for each of these structures and compared to PES measurements (Stadnik *et al* 1997). The lowest panel (d) shows the calculated SXES spectra for Ni 3d and Co 3d, respectively, for one atomic arrangement, that are compared to the corresponding experimental spectra (Fournée 1998).

The comparison with the SXES data allows for the selection of the best structural model for the approximant to the decagonal quasicrystalline Al–Co–Ni structure.

5. Conclusion

In this paper, we have briefly presented two techniques that probe occupied band states of solids that furthermore complement each other. These are the photoemission and x-ray emission spectroscopies, respectively.

The first technique carries both electronic and structural information. On the one hand, in integrated x-ray photoemission spectroscopy or ultra-violet photoemission spectroscopy (XPS and UPS), total valence band states are obtained modulated by photoemission cross sections. On the other hand, angle resolved photoemission spectroscopy (ARXPS or ARUPS according to whether incident x-ray or photons are used to excite the spectra) gives information on energy bands and Fermi surface mapping. The other technique, so called SXES (soft x-ray emission spectroscopy) provides information on the electronic state distributions of a selected angular momentum around each component of a solid, and therefore gives partial local information on the electronic structure. Several examples of results obtained with these various techniques have been presented for the sake of illustration. Emphasis has been put on the complementarity of integrated photoemission and soft x-ray spectroscopies through selected examples, although in these cases the SXES spectra have been obtained in the laboratories and not at synchrotron beam lines. The aim was to underline that to settle SXES spectrometers at synchrotron facilities may certainly be highly of interest as this technique can provide useful genuine information on the electronic structure of solids.

References

Agarwal B K 1979 *X-Ray Spectroscopy (Optical Series S987)* (Berlin: Springer)

Barr T L 1993 *Modern ESCA. The Principles and Practice of X-Ray Photoelectron Spectroscopy* (Boca Raton, FL: Chemical Rubber Company)

Belin-Ferré E, Dankhazi Z, Fournée V, Sadoc A, Berger C, Müller H and Kirchmayr H 1996 *J. Phys.: Condens. Matter* **8** 6213

Bonnelle C 1987 *R. Soc. Chemistry of London Annual Report* C, p 201

Brundle C R and Baker A D 1978 *Electron Spectroscopy. Theory, Techniques and Applications* (London: Academic)

Burdick G A 1963 *Phys. Rev.* **129** 138

Cardona M and Ley L 1978/1979 *Photoemission in Solids (Topics in Applied Physics 26, 27)* (Berlin: Springer)

Carlisle J A, Shirley E L, Terminello L S, Jia J J, Calcott T A, Ederer D L, Perera R C L and Himpsel F J 1999 *Phys. Rev.* B **59** 7433

Cole R J, Evans J A, Duo L, Laine A D, Fowles P S, Weightman P, Mondio G and Norman D 1992 *Phys. Rev.* B **46** 3474

Fournée V 1998 *Thesis* University Paris IV

Fournée V, Belin-Ferré E and Dubois J M 1998 *J. Phys.: Condens. Matter* **10** 4231

Fuggle J C 1983 *J. Less Common Met.* **93** 159

Gallet J J, Mariot J-M, Journel L, Hague C F, Kappler J-P, Schmerber, Singh D J, Krill G, Goulon J and Rogalev A 1998 *Phys. Rev.* B **57** 7835

Gheorghiu de La Rocque A, Belin-Ferré E, Fontaine M-F, Sénémaud C, Olivier-Fourcade J and Jumas J-C 2000 *Phil. Mag.* B **80** 1933–42

Hague C F, Mariot J-M, Strange P, Durham P J and Gyorffy B L 1993 *Phys. Rev.* B **48** 3560

Hüfner S 1995 *Photoelectron Spectroscopy* 2nd edn (Berlin: Springer)

Krajci M, Hafner J and Mihalkovic M 2000a *Phys. Rev.* B **62** 243–55

——2000b *Mater. Sci. Eng.* A **294–296** 548–52

Krajci M, Windisch M, Hafner J, Kressen G and Mihalkovic M 1995 *Phys. Rev.* B **51** 17 355

Krause M O and Oliver J H J 1979 *Phys. Chem. Ref. Data* **8** 329

Lindau I and Spicer W E 1974 *J. Electron Spectrosc.* **3** 409

Ma Y, Wassdahl N, Skytt P, Guo J, Nordgren J, Johnson P D, Rubensson J-E, Boske T, Eberhardt W and Kevan S D 1992 *Phys. Rev. Lett.* **69** 2598
Powell C J 1974 *Surf. Sci.* **44** 29
Rossi G, Lindau I, Braicovich L and Abbati I 1983 *Phys. Rev.* B **28** 3031
Siegbahn K *et al* 1967 *Nova Acta Regiae Soc. Sci. Ups.* **4** 20
——1969 *ESCA: Applied to Free Molecules* (Amsterdam: North-Holland)
Sonder A 1990 *Thesis* Paris IV
Speier W, van Leuken E, Fuggle J C, Sarma D D, Kumar L, Dauth B and Buschow K H J 1989 *Phys. Rev.* B **39** 6008
Stadnik Z M and Stroink G 1993 *Phys. Rev.* B **47** 100
Stadnik Z M, Purdie D, Garnier M, Baer Y, Tsai A P, Inoue A, Edagawa K, Takeuchi S and Buschow K H J 1997 *Phys. Rev.* B **55** 10 938
Stadnik Z M, Zhang G W, Tsai A P and Inoue A 1995 *Phys. Rev.* B **51** 11 358
Trambly de Laissardière G, Dankhazi Z, Belin E, Sadoc A, Nguyen Manh D, Mayou D, Keegan M and Papaconstantopoulos D A 1995 *Phys. Rev.* B **51** 14 035
Weaver J H, Franciosi A and Moruzzi V L 1984 *Phys. Rev.* B **39** 6008
Weijs P J W, Czyzyk M T, Fuggle J C, Speier W, Sarma D D and Buschow K H J 1990 *Z. Phys.* B **78** 423
Yeh J J 1993 *Atomic Calculation of Photoionisation Cross-Sections and Asymmetry Parameters* (New York: Gordon and Breach)
Yeh J J and Lindau I 1985 *At. Data Nucl. Data Tables* **32** 1
Zhang G W, Stadnik Z M, Tsai A P, Inoue A and Miyazaki T 1995 *Z. Phys.* B **97** 439